Quantum structure and rotational dynamics of HCN in helium clusters

Alexandra Viel, K. Birgitta Whaley

Quantum structure and rotational dynamics of HCN in helium clusters

Alexandra Viel[a] and K. Birgitta Whaley[b]
Department of Chemistry and Kenneth S. Pitzer Center for Theoretical Chemistry, University of California, Berkeley, California 94720-1460

(Received 1 June 2001; accepted 8 August 2001)

We present diffusion Monte Carlo calculations of ground states and rotationally excited states of HCN ^4He_n, using our recently developed algorithm for importance sampled rigid body diffusion Monte Carlo [Viel *et al.*, Comput. Phys. Commun. (in press, 2001)] within the mixed frame implementation. Excited states are studied with both fixed node approximations, and the Projection Operator Imaginary Time Spectral Evolution (POITSE) method that allows nodal constraints to be circumvented. Improvements in the POITSE algorithm allow excited states of clusters with up to 80 degrees of freedom to be determined here. The results presented here show that the rotational dynamics of the HCN molecule in ^{4}He clusters are very different from the behavior of heavier molecules such as SF_6. Detailed analysis of ground state densities shows that the lighter HCN molecule induces negligible adiabatic following of the helium density as a result of its rotational motion. The excited state calculations show that for small numbers of ^{4}He atoms the nodal structure does not correspond to that of a freely rotating molecule. Nevertheless, the POITSE calculations indicate that there is some admixture of this nodal structure in the low-lying rotational excitations. It is found that a relatively large number of ^{4}He atoms are required to achieve saturation of the effective rotational constant at the experimental value, in contradistinction to the small numbers of atoms required to saturate the rotational constant for heavier molecules such as SF_6 and OCS. © *2001 American Institute of Physics.* [DOI: 10.1063/1.1407270]

I. INTRODUCTION

An increasing number of experimental studies of helium clusters doped with atoms and molecules are now being performed,[1,2] driven by the recognition that such studies can lead to microscopic understanding of superfluid properties, as well as to novel quantum phenomena due to the quantum solvation of a strongly bound impurity provided by a superfluid. One of the most striking features to emerge from spectroscopic studies is the phenomenon of free rotation for embedded molecules in clusters of ^{4}He, the bosonic isotope of helium.[3] Rotational spectra measured with infrared or microwave spectroscopy for a series of molecules possessing gas phase rotational constants B_0, in the range 0.01–50 cm^{-1},[1,3] appear to fall into two dynamical regimes. The heavier molecules ($B_0 \leqslant 0.1\,cm^{-1}$) show a reduction in rotational constant of ~60%–80%, while lighter molecules show a much smaller reduction of 0%–30%. The HCN molecule lies in the latter regime, with gas phase $B_0 = 1.47\,cm^{-1}$ and a reduction of 19% in ^{4}He clusters to an effective B value of 1.20 cm^{-1}. Measurements come from two different experimental groups, and show a slight dependence on vibrational state of C–H stretching ($B = 1.204\,cm^{-1}$ for $v = 0$,[4] and 1.174 cm^{-1} for $v = 1$, Ref. 5). The isotopically substituted DCN molecule has also been studied, and shows a very similar decrease in rotation constant, 17% for $v = 0$.[4] These 17%–19% reductions are significantly less than the ~67% decrease observed for the heavier molecules, SF_6 (Ref. 6) and OCS.[7]

For the heavier molecules, one of us has proposed the notion of adiabatic following of the molecular rotation by part of the helium density.[3,8] Detailed microscopic quantum analysis has shown that while *total* adiabatic following by the helium density is not justified for these molecules, some degree of adiabatic following is nevertheless justified.[3] This has enabled simple dynamical models for the response of the locally inhomogeneous superfluid to rotation of the microscopic molecular probe to be developed.[3] The most sophisticated of these is a two-fluid model based on the identification of a local molecular-interaction induced nonsuperfluid density that coexists with the local superfluid density in the first solvation shell[9] and that may adiabatically follow the molecular rotation in certain cases, leading to an increase in the effective moment of inertia.[3] Such dynamical models, based on microscopic densities calculated with path integral[9] or density functional[10] techniques, complement the direct analysis of rotational constants via explicit energy level calculations using diffusion Monte Carlo techniques.[8] Together, the path integral and diffusion Monte Carlo based approaches have provided a complete and consistent analysis of the quantum rotational dynamics of heavy molecules such as SF_6 in ^{4}He clusters.[3]

In contrast, much less is understood about the dynamical behavior of the lighter molecules in helium clusters. The HF molecule has been studied in the ground rotational state, and the extreme isotropy of the helium density around this was taken to suggest that the rotational constant of this molecule would not be affected by the superfluid solvation.[11] This theoretical prediction has recently been confirmed by the measurement of only a 2% reduction in rotational constant for

[a]Electronic mail: viel@holmium.cchem.berkeley.edu
[b]Electronic mail: whaley@socrates.berkeley.edu

HF ($v=1$) in ^{4}He droplets.[12] HF thus appears to provide an extreme calibration point of a light molecule possessing a relatively weak interaction with helium (well depth ~ 40 cm^{-1}, Ref. 13), where the large zero point effects remove the dynamical consequences of the potential anisotropy. As pointed out in Ref. 11, the ground state energy of HF–He lies at -7.50 cm^{-1}, well above the height of the barrier at -18.0 cm^{-1} that separates the two minima. HCN is a very interesting molecule to compare with this extreme reference in the regime of lighter molecules. Like HF it is also linear. It possesses a somewhat shallower interaction with helium (well depth ~ 30 cm^{-1}, Ref. 14) than does HF, but is heavier than HF. The ground state of HCN–He lies at -9.65 cm^{-1}, which is now only just above the energy of the potential barrier at -11.7 cm^{-1}. This leads one to expect a more complex quantum rotational motion, with greater evidence of hindrance due to the potential anisotropy. The fact that it shows a much larger reduction in rotational constant than HF ($\sim 19\%$ compared with $\sim 2\%$), provides experimental evidence that HCN possesses considerably more complex quantum dynamical rotational motion in helium.

Prior to this work, no theoretical studies of the quantum rotational motion of HCN in helium clusters have been made. However, classical energetic estimates employing path integral densities[3] have indicated that there can be no adiabatic following for HCN. In addition, a scaling of the quantum analysis made for SF_6 to lighter spherical top rotors showed that adiabatic following by the helium density is absent for fast rotors having rotational constants similar to HCN.[8] The focus of this paper is to now provide a thorough microscopic quantum analysis of the rotational dynamics of HCN in helium clusters, employing fully quantum calculations incorporating the rotational motion of the HCN molecule in addition to all van der Waals degrees of freedom. Ground state energies and structures are determined for a range of cluster sizes varying from $n=1$ to $n=60$ using our recently developed importance sampled rigid body diffusion Monte Carlo algorithm.[15] Comparison of ground state structures obtained with and without molecular rotation allows us to demonstrate a lack of adiabatic following by the helium. Excited states are then calculated using both a fixed node approximation and an intrinsically exact method, POITSE, that relaxes nodal approximations. Energy differences between $J=1$ and $J=0$ levels are used to extract the effective rotational constant B, and the variation of this with cluster size is analyzed. We find that the HCN molecule shows a surprisingly rich rotational dynamic behavior inside bosonic ^{4}He clusters. This behavior is in many respects considerably more complex than the corresponding rotational dynamics of heavier molecules such as SF_6 and OCS. We suggest here that this behavior is related to the lack of adiabatic following of helium with the HCN rotation, together with strong quantum coupling effects introduced by the close proximity of the zero point energy to the potential barrier in the HCN–He system.

In Sec. II we briefly summarize the various diffusion Monte Carlo methods used here, providing the relevant critical modifications of the importance-sampled rigid body DMC and POITSE algorithms that were necessary for successful study of the He_n HCN system. Results and discussion are presented in Sec. III, and the dynamical behavior of HCN summarized and put in context of other molecules in Sec. IV.

II. THEORETICAL APPROACH

A. Monte Carlo techniques

The only methods currently available for studying quantum system with many degrees of freedom (>6) are based on stochastic techniques such as the variational and diffusion Monte Carlo (VMC and DMC) methods. In this paper, we employ rigid body diffusion Monte Carlo (RBDMC), implementing importance sampling of all degrees of freedom, according to our recently developed general formalism.[15] RBDMC is combined here for the first time with the projection operator imaginary time spectral evolution (POITSE) methodology for calculation of excited states without nodal approximations.[16,17] To date, the POITSE method has been used for the calculation of excited states for system with up to 15 dimensions.[18,19] We present here a modified implementation of the POITSE scheme which allows us to now study rotational excitation of systems with significantly larger dimensionality, i.e., ~ 80 degrees of freedom (see also Refs. 20 and 21). The basic VMC and DMC methodology has been described in many papers.[2,22–26] Therefore we provide here only a brief description of the basic approach, focusing instead on description of the above algorithmic developments in RBDMC and POITSE that were necessary for successful treatment of the HCN molecule in helium clusters, in addition to the specific details of the calculations for HCN.

1. Variational diffusion Monte Carlo: VMC

Variational Monte Carlo was used in this work to optimize trial wave functions needed for diffusion Monte Carlo, and to create the initial configurations for the POITSE calculations. In this simplest stochastic approach to solution of the Schrödinger equation, one approximates the expectation value for a coordinate operator $\hat{O}(\mathcal{R})$ over $\Psi_T(\mathcal{R})$ by

$$\frac{\int \Psi_T^*(\mathcal{R})\hat{O}(\mathcal{R})\Psi_T(\mathcal{R})d\mathcal{R}}{\int |\Psi_T(\mathcal{R})|^2 d\mathcal{R}} \simeq \frac{1}{M}\sum_{i=1}^{M} \hat{O}(\mathcal{R}_i) = \langle \hat{O} \rangle_{\mathrm{VMC}}, \tag{1}$$

where $\mathcal{R}$ is a vector describing the coordinate space configuration of the system, M is the number of configurations which are sampled from the distribution $P(\mathcal{R})=|\Psi_T(\mathcal{R})|^2$ via a Metropolis algorithm.[27] The optimization of the parametrized trial wave function is done by computing the average for the Hamiltonian operator and by minimizing either the energy or its variance.[28] Our implementation of VMC here was made using an unbiased random walk where each element k of the vector $\mathcal{R}$ moves inside an interval $[-\zeta_k, \zeta_k]$. The box sizes are chosen such that the number of accepted moves is approximately maintained at half the number of attempted ones. The index k refers to the different kinds of degrees of freedom as we explain below. All box sizes ζ_k are taken to be equal, after checking that taking different values for different degrees of freedom had no significant effect on the results.

2. Unbiased and biased RBDMC

In the diffusion Monte Carlo scheme, the time-dependent Schrödinger equation is rewritten introducing the imaginary time $\tau = it/\hbar$:

$$\frac{\partial \Psi(\mathcal{R})}{\partial \tau} = \sum_j^{\mathcal{N}} D_j \nabla_j^2 \Psi(\mathcal{R}) - [V(\mathcal{R}) - E_{\text{ref}}]\Psi(\mathcal{R}), \tag{2}$$

where $\mathcal{R}$ is now specifically a vector in the $\mathcal{N}$-dimensional space, $D_j = \hbar^2/2m_j$ if the jth degree of freedom corresponds to a translation, and $D_j = B_j = \hbar^2/2I_j$ if this degree of freedom corresponds to a rotation. In the above equation, E_{ref} is a constant defining the zero of the absolute energy scale, and V is the potential. This formulation implies the use of Cartesian coordinates for the atomlike particles and for the center of mass of the rigid body, and the use of rotational angles around the principal axes of the rigid body.

To improve the efficiency of this method and to make possible the study of large clusters incorporating weakly bound species like ^{4}He, one usually introduces a guiding function Ψ_T which approximates the true solution Ψ of Eq. (2). The introduction of this guiding function leads to a diffusionlike equation for the product function $f(\mathcal{R}) = \Psi(\mathcal{R})\Psi_T(\mathcal{R})$, that differs from Eq. (2) by the presence of additional drift terms:

$$\frac{\partial f(\mathcal{R})}{\partial \tau} = \sum_j^{\mathcal{N}} \{D_j \nabla_j^2 f(\mathcal{R}) - D_j \nabla_j [f(\mathcal{R}) F_j(\mathcal{R})]\} - [E_l(\mathcal{R}) - E_{\text{ref}}] f(\mathcal{R}). \tag{3}$$

Here $E_l(\mathcal{R}) = \Psi_T(\mathcal{R})^{-1} \hat{H} \Psi_T(\mathcal{R})$ is the local energy, and $F_j(\mathcal{R}) = \nabla_j \ln|\Psi_T(\mathcal{R})|^2$ is the quantum force that controls the drift terms.

A random walk technique is used to determine the steady state of Eq. (3) or Eq. (2). A walker (or configuration) is defined as a vector $\mathcal{R}$ in the $\mathcal{N}$-dimensional space. It represents the position and orientation of all the particles of the system under study. An ensemble of walkers is propagated from some arbitrary initial distribution using the short time approximation of the Green's function appropriate to Eq. (3):

$$G(\mathcal{R} \to \mathcal{R}'; \delta\tau) = \prod_j \left[\frac{1}{(4\pi D_j \delta\tau)^{1/2}} \times \exp\{-(\mathcal{R}_j' - \mathcal{R}_j - D_j \delta\tau F_j(\mathcal{R}))\} \times \exp\left\{ -\delta\tau_{\text{eff}} \left[\frac{E_l(\mathcal{R}) + E_l(\mathcal{R}')}{2} - E_{\text{ref}} \right] \right\} \right]. \tag{4}$$

The statistical representation of this Green's function takes two steps. First, each coordinate of the walkers is moved according to a Gaussian distributed random number characterized by a standard deviation of $\sqrt{2 D_j \delta\tau}$ and displaced by the quantum drift force $D_j \delta\tau F_j(\mathcal{R})$. Detailed balance is ensured by using a Metropolis scheme at each time step. According to this, the abovementioned attempted move from $\mathcal{R}$ to $\mathcal{R}'$ is accepted with probability

$$P(\mathcal{R} \to \mathcal{R}') = \min\left\{ 1, \frac{|\Psi_T(\mathcal{R}')|^2}{|\Psi_T(\mathcal{R})|^2} \frac{G(\mathcal{R}' \to \mathcal{R}; \delta\tau)}{G(\mathcal{R} \to \mathcal{R}'; \delta\tau)} \right\}. \tag{5}$$

This acceptance/rejection step requires us to define the effective time step $\delta\tau_{\text{eff}}$ of Eq. (4):

$$\frac{\delta\tau_{\text{eff}}}{\delta\tau} = \frac{1}{n_k} \sum_k \frac{\langle \Delta\mathcal{R}^2 \rangle_k^{\text{acc}}}{\langle \Delta\mathcal{R}^2 \rangle_k^{\text{att}}}. \tag{6}$$

Here k refers to different types of degrees of freedom, and n_k is the number of degrees of freedom controlled by the same D_j coefficient. The average $\langle \cdots \rangle_k$ only includes those degrees of freedom of type k, i.e., the different contributions from atom or rigid body translations, or from rigid body rotations. For the current study, $n_k = 3$, i.e., helium atom translations, HCN center of mass translation, and HCN rotations. For a cluster with n helium atoms, we have then

$$\frac{\delta\tau_{\text{eff}}}{\delta\tau} = \frac{1}{3} \left[\frac{\langle \Delta\varphi_x^2 + \Delta\varphi_y^2 \rangle^{\text{acc}}}{\langle \Delta\varphi_x^2 + \Delta\varphi_y^2 \rangle^{\text{att}}} + \frac{\langle \Delta x_{\text{HCN}}^2 + \Delta y_{\text{HCN}}^2 + \Delta z_{\text{HCN}}^2 \rangle^{\text{acc}}}{\langle \Delta x_{\text{HCN}}^2 + \Delta y_{\text{HCN}}^2 + \Delta z_{\text{HCN}}^2 \rangle^{\text{att}}} + \frac{\langle \Sigma_{j=1}^n \Delta x_j^2 + \Delta y_j^2 + \Delta z_j^2 \rangle^{\text{acc}}}{\langle \Sigma_{j=1}^n \Delta x_j^2 + \Delta y_j^2 + \Delta z_j^2 \rangle^{\text{att}}} \right], \tag{7}$$

where $\{x_i, y_i, z_i; i = 1,...,n\}$ refers to the Cartesian coordinates of the n helium atoms, $x_{\text{HCN}}, y_{\text{HCN}}, z_{\text{HCN}}$ refers to the Cartesian coordinates of the center of mass of HCN, and φ_x, φ_y refers to the angles of rotation in the principal axis frame (PAF) of HCN. This constitutes a mixed frame implementation of RBDMC, in contradistinction to the fixed frame implementation used previously for a spherical top molecule in helium clusters[8] (see discussion in Sec. II B 2 below). The DMC acceptance rates are around 99.99% in our calculations, with a slightly smaller value being achieved in excited state computations.

The last factor of the Green's function is implemented here through a branching scheme, whereby walkers can be kept, destroyed or replicated. Each walker is branched according to

$$M = \text{int}\left[\exp \delta\tau_{\text{eff}} \left(E_{\text{ref}} - \frac{E_l(\mathcal{R}) + E_l(\mathcal{R}')}{2} \right) + \zeta \right], \tag{8}$$

where ζ is a uniformly distributed random number. In order to keep a reasonable ensemble size, we update the reference energy by

$$E_{\text{ref}}^{\tau + \delta\tau} = E_{\text{ref}}^{\tau} + \frac{a}{\delta\tau} \ln\left[\frac{N(\tau)}{N(\tau + \delta\tau)} \right], \tag{9}$$

where N is the ensemble size, and a is a parameter. This parameter was arbitrarily chosen for equilibration of the configurations. For production runs, it was then reduced to a value that results in a similar variance for $\langle E_{\text{ref}} \rangle$ and for $\langle E_l \rangle$. Other implementations based on continuous weights can be used. A pure DMC scheme is usually less numerically stable[29] and has to be supplemented by branching steps.[30,31]

The energy of the system can be computed as the average of the local energy $E_l(\mathcal{R})$ or of the reference energy E_{ref}. The difference between these two estimates provides a measure of the actual time step error introduced by both use of a trial wave function (usually linear), and by the short

time representation of the Green's Function [$\mathcal{O}(\delta\tau^2)$ for $\Psi_T=1$].[31] In this article, we report the average of the local energy, since the average of the reference energy was always found to be equal to this within the error bars.

3. Fixed node approximation

The computation of excited state energies is not an easy task with DMC. The fixed node approximation enables one to compute excited state levels by imposing a predefined nodal surface. Practical implementation of this approximation consists in adding a rejection step in the scheme. Thus at each time step, any attempted move that crosses the nodal surface is rejected, and the walker keeps its former position. The use of a guiding function with a nodal structure can make the DMC walk considerably more difficult to stabilize. Indeed, we have found that close to the node, the drift term can be extremely large, resulting in the creation of ''persistent'' walkers.[24] Those configurations are stuck at positions close to the node where the local energy is not always accurate. This problem was overcome by first reducing the time step, and second by using a modified version of the quantum force:[24,32]

$$F_j(\mathcal{R})_{\text{modified}}=\frac{-1+\sqrt{1+2D_j[F_j(\mathcal{R})]^2\delta\tau}}{D_j[F_j(\mathcal{R})]^2\delta\tau}F_j(\mathcal{R}). \quad (10)$$

This has a smoother behavior close to nodes, since it does not assume that F_j is constant, but only ΔF_j.

The position of the nodal surfaces was checked here by propagating two different ensembles, each one restricted to be in one side of the node. This scheme allows us to optimize the node position by requiring that the two one-sided energies be equal.[33] This simple check of the nodal position is not an absolute criterion in any other than one dimension, and one must therefore bear in mind that the fixed node results are implicitly dependent on the nodal surface chosen. In the studies described here, we shall analyze and compare the excited state results obtained from three different nodal surfaces for the $n=1$ He–HCN ''dimer.'' It is important to recognize that the accuracy of a given nodal approximation has nothing to do with the specific implementation of the RBDMC, i.e., whether mixed or fixed frame is used.

4. Expectation values

One of the attractive features of Monte Carlo methods is that it provides geometrical information on the system since one has access to either the full-dimensional wave function (unbiased DMC) or to the product $\Psi\Psi_T$ (biased DMC). Arbitrary property expectation values are computed by replacing integrals by sums over samples. In particular, this technique can be applied to positional functions which are very useful in visualizing the structure of the clusters such as the radial distribution of helium atoms relative to the center of mass of the HCN molecule

$$P_{\text{rad}}(R)=\frac{1}{n}\sum_{i=1}^{n}\left\langle\frac{\delta(R_i-R)}{R^2}\right\rangle_{\text{walk}}, \quad (11)$$

and the angular density distribution $\rho(r,z)$ of helium atoms with respect to the HCN molecule

$$\rho(r,z)=\frac{n}{2\pi}\sum_{i=1}^{n}\left\langle\frac{\delta(r_i-r)}{r}\delta(z_i-z)\right\rangle_{\text{walk}}, \quad (12)$$

where the z axis is defined by the HCN molecule, and r is the distance to this axis.

Since importance sampling is employed, we obtain the mixed averages $\langle\Psi|\hat{O}|\Psi_T\rangle$. To obtain the true average over Ψ, these should be corrected by multiplying with the factor Ψ/Ψ_T in the integrand. This can in principle be obtained by descendant weighting.[34] Alternatively, we can use the extrapolated quantity $2\langle\Psi|\hat{O}|\Psi_T\rangle-\langle\Psi_T|\hat{O}|\Psi_T\rangle=\langle\Psi|\hat{O}|\Psi\rangle+\mathcal{O}(\Delta\Psi^2)$, where $\Delta\Psi=\Psi-\Psi_T$. This is correct to second order in the difference $\Delta\Psi$. We present here only mixed densities $\rho_{\text{mixed}}\equiv\langle\Psi|\hat{\rho}|\Psi_T\rangle$. These provide an adequate representation of the rotational features that we are interested in demonstrating in this work.

5. Projection operation imaginary time spectral evolution (POITSE)

The computation of excited state energies using a fixed node approximation requires some knowledge of the nodal structure of the excited state. The use of incorrect nodes can lead to incorrect values of the energies, as we will show explicitly later. The POITSE scheme overcomes this approximation and can yield exact excited state energies.[16] In this scheme, one extracts excited state energies from the two-sided inverse Laplace transform of an imaginary time correlation function $\tilde{\kappa}(\tau)$. The time-dependent decay of this correlation function is computed using a multi-dimensional Monte Carlo integration, combined with zero temperature diffusion Monte Carlo sidewalks.[16] In imaginary time, the correlation function will eventually decay as the sidewalks provide relaxation to the initial state, usually taken to be an approximation to the ground state. The basic idea is then to study the behavior of the Green's function at small imaginary times, before the equilibration to the ground state distribution is completed, and to thereby extract information about the excited states. The decay of the correlation, $\tilde{\kappa}(\tau)$ contains information about energy differences E_f-E_0, where E_0 is the ground state energy and E_f an excited state energy level. Specifically, $\tilde{\kappa}(\tau)$ can be transformed to yield an excitation function from which the excitation energies can simply be read off. The transformation is performed here with the maximum entropy method, as described in Ref. 16.

The renormalized POITSE correlation function can be written[16] in a convenient form for Monte Carlo evaluation

$$\tilde{\kappa}(\tau)=\frac{\dfrac{\langle\Psi_T|A\exp[-(\hat{H}-E_0\tau]A^{\dagger}|\Psi_T\rangle}{\langle\Psi_T|\Psi_T\rangle}}{\dfrac{\langle\Psi_T|\exp[-(\hat{H}-E_0)\tau]|\Psi_T\rangle}{\langle\Psi_T|\Psi_T\rangle}}. \quad (13)$$

In this equation, A is a local operator chosen to project from the trial function $|\Psi_T\rangle$ onto some excited state $|\Psi_f\rangle$. An inverse Laplace transform of $\tilde{\kappa}(\tau)$ yields to the desired spectral information $\kappa(\omega)$,

$$\kappa(\omega)=\sum_f|\langle\Psi_T|A|\Psi_f\rangle|^2\delta(E_0-E_f+\omega). \quad (14)$$

Former implementations of this scheme were made using sidewalk DMC propagations inside a variational Monte Carlo outer loop.[16–19] The sidewalk DMC propagations were done using continuous weights and a constant size for the ensemble of walkers. The use of weights instead of branching is appealing since the evaluation of $\tilde{\kappa}(\tau)$ is thus simple.[16]

In general, DMC propagations with weights are known to be unstable, because after some time the distribution of weights among the walkers is unequal and some walkers carry all the weights, whereas some carry very small weights. This feature can have a drastic effect on a POITSE scheme, since if the energy difference we are looking at is small, the length of the sidewalks need to be increased and one may then reach the region of instability. This has limited use of POITSE to $\leqslant 15$ dimensions to date. We have overcome this difficulty here by using DMC sidewalks with pure branching. (Related studies are now being carried out using a combination of weights and branching.[20,21]) In this pure branching formulation, the number of walkers is not kept constant and is instead a function of τ, $N(\tau)$. The new expression for $\tilde{\kappa}(\tau)$ is given by

$$\tilde{\kappa}(\tau)=\frac{1}{N(\tau)}\sum_{k=1}^{N(\tau)} A^{\dagger}(\mathcal{R}_{j(k)}^{(0)})A(\mathcal{R}_{k}^{(\tau)}), \tag{15}$$

where $j(k)$ gives the ''ascendant'' of the current walker k, i.e., the index of the initial walker at $\tau=0$, from which the walker k at time τ comes from because of branching. The initial configuration $\mathcal{R}_k^{(0)}$ is distributed according to Ψ_T^2, thanks to the VMC outer loop.

In order to compute the rotational excitation of HCN inside helium clusters we employ here a projector composed of the molecular $J=1$, $M=0$, $K=0$ Wigner function in the space fixed frame. This projector is a function only of the second Euler angle that specifies the orientation of the molecular frame in the (arbitrary) space fixed frame. We emphasize that the projector provides only a kind of initial guess for the nodal structure of the excitations, and that these are modified as the sidewalks proceed. Indeed, it is instructive to compare the excitation energies obtained using the nodal structure of the projectors within a fixed node approximation, with the results from a full POITSE calculation. We shall do this for the rotational excitation of HCN–He in Sec. III below, and will see that they can produce very different results.

B. Description of the system

The system considered in the present study is made of n helium atoms and one rigid linear HCN molecule.

1. Potential

All the calculations were made with a purely pairwise-additive potential energy surface based on *ab initio* calculation and spectroscopic data for He–HCN components, and employing the HFD–B potential of Aziz *et al.*[35] for the He–He interaction. The He–He potential is an isotropic function of the distance between the two helium atoms. For He–HCN, we use the 1E8 potential of Atkins and Hutson.[14] This potential is expressed as a function of the Jacobi coordinates (R, θ) of He with respect to the linear HCN molecule. The geometry of the minimum is linear, with He situated close to the H atom at a distance of $R_{\mathrm{He-HCN}}=4.2$ Å from the center of mass of HCN. The overall potential energy of the He_nHCN cluster is thus:

$$V(\mathcal{R})=\sum_{j=1}^{n} V^{\mathrm{HeHCN}}(R_j,\theta_j)+\sum_{j<k}^{n} V^{\mathrm{HeHe}}(R_{jk}), \tag{16}$$

where R_{jk} is the distance between two helium atoms. Because the HCN–He potential well is considerably deeper than the He–He well (29.6 cm^{-1} relative to 7.5 cm^{-1}) and the binding energy of HCN–He is also much larger [9.66 cm^{-1} (Refs. 15,36) relative to $\sim 10^{-3}\,\mathrm{cm}^{-1}$ (Ref. 37)], the HCN molecule is located inside the He_n cluster and not at the surface of the He_n component.

2. Hamiltonian

In the calculations presented here, we implicitly use the Born–Oppenheimer approximation in order to separate the electronic motion from the nuclear one. These studies focus on the van der Waals degrees of freedom, for which the typical time scale is well separated from the internal degrees of freedom of HCN. Therefore, we can treat the HCN molecule as a rigid body. The kinetic term in the Hamiltonian of the cluster consists of translational and rotational terms. Contrary to basis set expansion methods, we do not try to separate out the overall translation and rotation of the whole system here, since this will only eliminate 6 or 5 degrees of freedom, at the expense of making the DMC considerably more complicated. The translational part is expressed using the Cartesian coordinates of each particle, i.e., the n helium atoms and the HCN center of mass. The entire cluster is thus allowed to translate and rotate during the calculation. The rotation of the rigid HCN has a simple expression when the principal axis frame of HCN is used. The full Hamiltonian is given by

$$\hat{H}(\mathcal{R})=-\sum_{j=1}^{n}\frac{\hbar^2}{2m}\left\{\frac{\partial^2}{\partial x_j^2}+\frac{\partial^2}{\partial y_j^2}+\frac{\partial^2}{\partial z_j^2}\right\}-\frac{\hbar^2}{2M}\left\{\frac{\partial^2}{\partial X^2}+\frac{\partial^2}{\partial Y^2}+\frac{\partial^2}{\partial Z^2}\right\}-B_0\left\{\frac{\partial^2}{\partial \varphi_x^2}+\frac{\partial^2}{\partial \varphi_y^2}\right\}, \quad +V(\mathcal{R}) \tag{17}$$

where m is the mass of ^{4}He, M the mass, and B_0 the rotational constant, respectively, of HCN. In this equation, φ_x and φ_y correspond to rotations around the principal axes **x** and **y** of HCN. In the particular case of a linear rotor like HCN, the PAF is defined by its z axis which is taken to be along the molecular axis. The x and y axes are two arbitrary axes perpendicular to this. We define all the Cartesian coordinates in the laboratory (or space fixed) frame. The combination of laboratory and principal axis frame coordinates summarized in Eq. (17) provides a mixed frame implementation of the rigid body DMC.[15] Such a mixed frame implementation is essential for multiple rigid body simulations. For a single linear molecule interacting with many helium atoms, one could in principle also use a fixed frame implementation in the PAF of this molecule. However, the mixed frame implementation possesses

TABLE I. Parameters used for the anisotropic and radial trial wave functions, Eqs. (21) and (25).

	a_0	a_1	a_2	a_3	c_0	c_1	c_2	c_3
				Anisotropic				
He HCN	0.747	0.0375	0.112	0.0966	16 850	−6825	46540	21 190
				Radial				
He HCN	0.638				22 067			
He He	0.006				3852			

the advantage of generality and is therefore the approach of choice here. In our calculations we use the helium and molecular parameters $m=4.002\,60$ amu, $M=27.011\,04$ amu, and $B_0=1.478\,221\,834\,\mathrm{cm}^{-1}$.

3. Trial wave functions

An overall form of ground state trial function that respects the Bose symmetry is given by the product of pair correlation terms[2]

$$\Psi_T(\mathcal{R})=\prod_{p=1}^{n}\Phi_T(R_k,\theta_k)\prod_{p\neq q}^{n}\Xi_T(R_{pq}). \tag{18}$$

We have made use of two different trial functions for the He–HCN interaction. The first one contains both a radial dependence R and an angular dependence θ, whereas the second one is purely radial. In order to have an approximate description of the ground state wave function of the He–HCN system, we choose to solve the Schrödinger equation of a reduced dimensionality problem. In particular, we solved the following radial equation:

$$-\frac{\hbar^2}{2\mu}\frac{\partial^2}{\partial R^2}\phi(R;\theta_q)+V^{\mathrm{HeHCN}}(R;\theta_q)\phi(R;\theta_q)=E(\theta_q)\phi(R;\theta_q) \tag{19}$$

for a series of θ_q values. This equation is the Schrödinger equation for a helium atom moving with a fixed orientation with respect to a fixed HCN molecule. In this equation μ is the reduced mass of the He–HCN system. In the above equation, we implicitly decouple the stretching and the bending mode, as well as the effect of the rotation of the HCN molecule. For this reason, in order to get useful trial functions, instead of using the real reduced mass of the system we employ a lighter mass, in order to make sure that the trial wave function obtained from Eq. (19) is broader than the full-dimensionality exact ground state function. We solve this series of one-dimensional equations by a standard collocation scheme based on sine functions and a regularly spaced grid.[38] The eigenfunctions are then fit to a simple exponential form

$$f(R)=b\exp\left(-\frac{c}{R^5}-aR\right), \tag{20}$$

where a and c are parameters, and b is a normalization factor. By using $b^{-1}=f((5c/a)^{1/6})$, we ensure that the maximum of this function is unity. The parameters a and c are functions of the angle θ_q, and are fit by a polynomial expression up to the third degree. All values of the parameters are presented in Table I. We add another angular dependence in the final two-dimensional function, since the maximum of the wave function is not constant as θ varies. The final expression for the trial function $\Phi_T(R,\theta)$ is then given by

$$\Phi_T(R,\theta)=[d_0+d_1\cos(\theta)]\frac{\exp\left(-\frac{c(\theta)}{R^5}-a(\theta)R\right)}{\exp\left(-\frac{c(\theta)}{R_0(\theta)^5}-a(\theta)R_0(\theta)\right)}, \tag{21}$$

$$R_0(\theta)=\left[\frac{5c(\theta)}{a(\theta)}\right]^{1/6}, \tag{22}$$

$$a(\theta)=a_0+a_1\theta+a_2\theta^2+a_3\theta^3, \tag{23}$$

$$c(\theta)=c_0+c_1\theta+c_2\theta^2+c_3\theta^3. \tag{24}$$

Optimization of this trial function was carried out by a series of variational Monte Carlo computations. We first varied the reduced mass μ, and checked that both the variational energy and the shape of the wave function are in agreement with the DMC results. We then included the extra angular dependence through parameters d_0 and d_1. The VMC energies and test DMC runs showed that adding such an angular dependence does not lead to either a large decrease of the VMC energy, nor to a big reduction in the statistical noise. We therefore employ the simplest combination of parameters d_i; $d_0=1$, and $d_1=0$. The introduction of this guiding function $\Psi(R,\theta)$ allows us to use a bigger time step (i.e., 50 a.u.) than is possible with unbiased DMC (i.e., 10 a.u.), and also reduces the statistical noise.

In order to study larger clusters with $n\sim 2,...,60$, we do not try to optimize this angular wave function. Instead, we define a simpler radial wave function of the form

$$\Phi_T^{\mathrm{rad}}(R)=\exp\left(-\frac{c_0}{R^5}-a_0R\right), \tag{25}$$

which is cheaper to evaluate. We performed several unbiased DMC runs and used the projection of the effective one-particle wave function in order to define the parameters a_0 and c_0. We fit $\Phi_T^{\mathrm{rad}}(R)$ to the radial projection for the largest cluster that we can study with unbiased DMC ($n=9$), raised to the power 0.8. The use of this power of 0.8 ensures that the fit will be broader than the real distribution, and thus will ensure sampling of all the relevant configuration space for large clusters.[15] The fitted parameter values obtained with Eq. (25) for $n=9$ are $a_0=0.638$ and $c_0=22\,067$. For the trial wave function component describing the He–He correlation

TABLE II. Ground state energies for HCN He_n, reported in cm^{-1}. The energies shown in the third and fourth columns were obtained with importance sampling DMC, employing the radial trial wave function, Eq. (25).

n	$\langle E\rangle_{\text{unbiased}}$	$\langle E\rangle$	$\langle E\rangle/n$
1	-9.7 ± 0.8	-9.71 ± 0.13	-9.71 ± 0.13
2	-19.7 ± 1.2	-19.72 ± 0.28	-9.86 ± 0.14
3	-30.1 ± 1.6	-29.90 ± 0.17	-9.67 ± 0.06
4	-40.3 ± 2.0	-40.15 ± 0.15	-10.02 ± 0.04
6	-60.6 ± 3.1	-60.61 ± 0.15	-10.10 ± 0.03
8	-80.9 ± 3.5	-81.19 ± 0.16	-10.15 ± 0.02
9	-90.3 ± 5.1		
10	-88.4 ± 5.6[a]	-101.3 ± 0.9	-10.13 ± 0.09
15		-142.8 ± 1.6	-9.52 ± 0.11
20		-164.8 ± 1.8	-8.24 ± 0.09
30		$-199. \pm 3.0$	-6.6 ± 0.1
40		$-233. \pm 5.0$	-5.8 ± 0.2
60		$-293. \pm 8.0$	-4.9 ± 0.2

[a]The unbiased energy for HCN He_{10} is unphysical since at this size one of the helium atoms dissociates unless importance sampling is employed.

$\Xi(R)$, we took a radial expression of the same form as Eq. (25). The corresponding parameters a_0 and c_0 reported in Table I were defined by fitting to the He–He eigenfunction obtained by a FBR-DVR calculation. A comparison with wave functions given in the literature[30,39] shows that the corresponding wave function used in this work is indeed much broader, as desired.

The excited state trial functions used in the fixed node calculations are constructed by multiplying the nodeless ground state function $\Psi_T(R)$ by a function that imposes the nodal structure. Thus,

$$\Psi_T^{(e)}(R)=\Psi_T^{(0)}(R)\Psi_{\text{node}}^{(i)}. \tag{26}$$

Three forms of nodal functions $\Psi_{\text{node}}^{(i)}$ are discussed in detail in Sec. III B below.

III. RESULTS

A. Ground state studies

We present first a systematic study of the ground state properties, using both unbiased and biased DMC. We found that unbiased DMC was unsuitable for the study of clusters with more than $n=9$ helium atoms, since the unphysical ''dissociation'' of helium atoms starts at that size.[15] The unbiased calculations are nevertheless required since they allow us to define the parameters of the radial trial wave function as described above. Table II summarizes the ground state energies. We employed the radial trial wave function for the importance sampling DMC calculations, which leads to a significant net reduction of the statistical noise. In order to estimate the statistical noise, we split the DMC propagation into blocks of a size longer than the correlation length. The square root of the variance computed using one energy per block is reported as the error. The results on Table II correspond to one run of 800 blocks, each of which consists of 150 time steps. The energy per helium atom is constant at ~ -10 cm^{-1} up to 15 atoms, then it starts to increase, indicating that the second solvation shell begins to form. This is also noticeable in the radial profile (see Fig. 1).

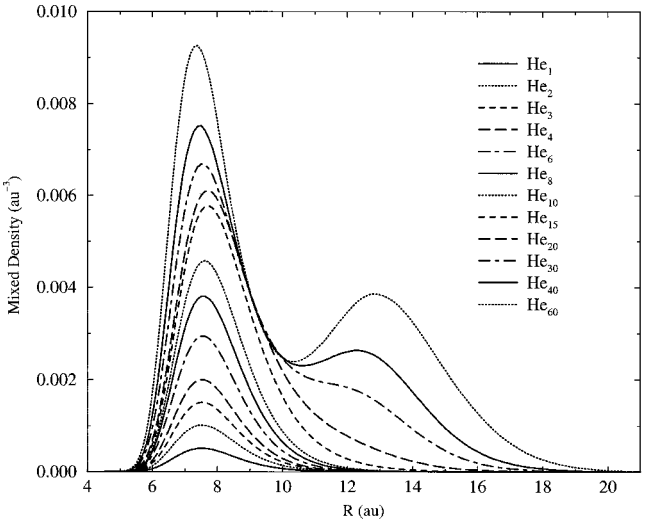

FIG. 1. Evolution of the mixed density radial profile with the number n of helium atoms. The curves are normalized such that $4\pi\int\rho_{\text{mixed}}(R)R^2dR=n$.

The mixed radial density profiles obtained with the radial trial wave function are presented in Fig. 1. The normalization was taken to be the number of helium atoms n. For sizes larger than $n\sim 20$ helium atoms, the second solvation shell starts to fill. For these larger clusters, the density maximum inside the first shell occurs closer to the HCN molecule. Such packing effects are general to all molecules in ^{4}He clusters, whether strongly bound[40] or weakly bound.[11]

As noted earlier, unbiased DMC gives access to the wave function of the system. We are thus able to see the effect of the rotation of HCN. The breakdown of the adiabatic following that was predicted for HCN by violation of an energetic criterion in Ref. 3 can be seen here by artificially suppressing the HCN rotation (i.e., setting $B_{\text{HCN}}\equiv B_0$ equal to zero) during the DMC propagation. The two corresponding wave function amplitudes, i.e., with and without molecular rotation, are presented in Fig. 2. Both plots show a maximum at the linear geometry corresponding to the He close to the H atom, which corresponds to the global minimum of the interaction potential. The wave function in the nonrotating case, Fig. 2(b) is much more localized than that for the physical system in which the HCN molecule rotates, Fig. 2(a). [Note that different scales were used for (a) and (b).] This localization is such that the probability to find the helium atom on the nitrogen side of the molecule is effectively zero, whereas it is finite for the real system. The large difference between those two amplitudes is a mark of very inefficient adiabatic following of the molecular rotation by the helium.[3] For complete adiabatic following, the helium wave function would be independent of the rotational state of the molecule, and of the presence of any molecular rotational kinetic energy. A more quantitative study of the extent of adiabatic following for various molecules will be published elsewhere.[41] The reduction of the rotational constant for HCN inside helium clusters can therefore not be explained by a model based on adiabatic following by any fraction of the helium density.[3]

Figure 3 shows the mixed densities for larger clusters,

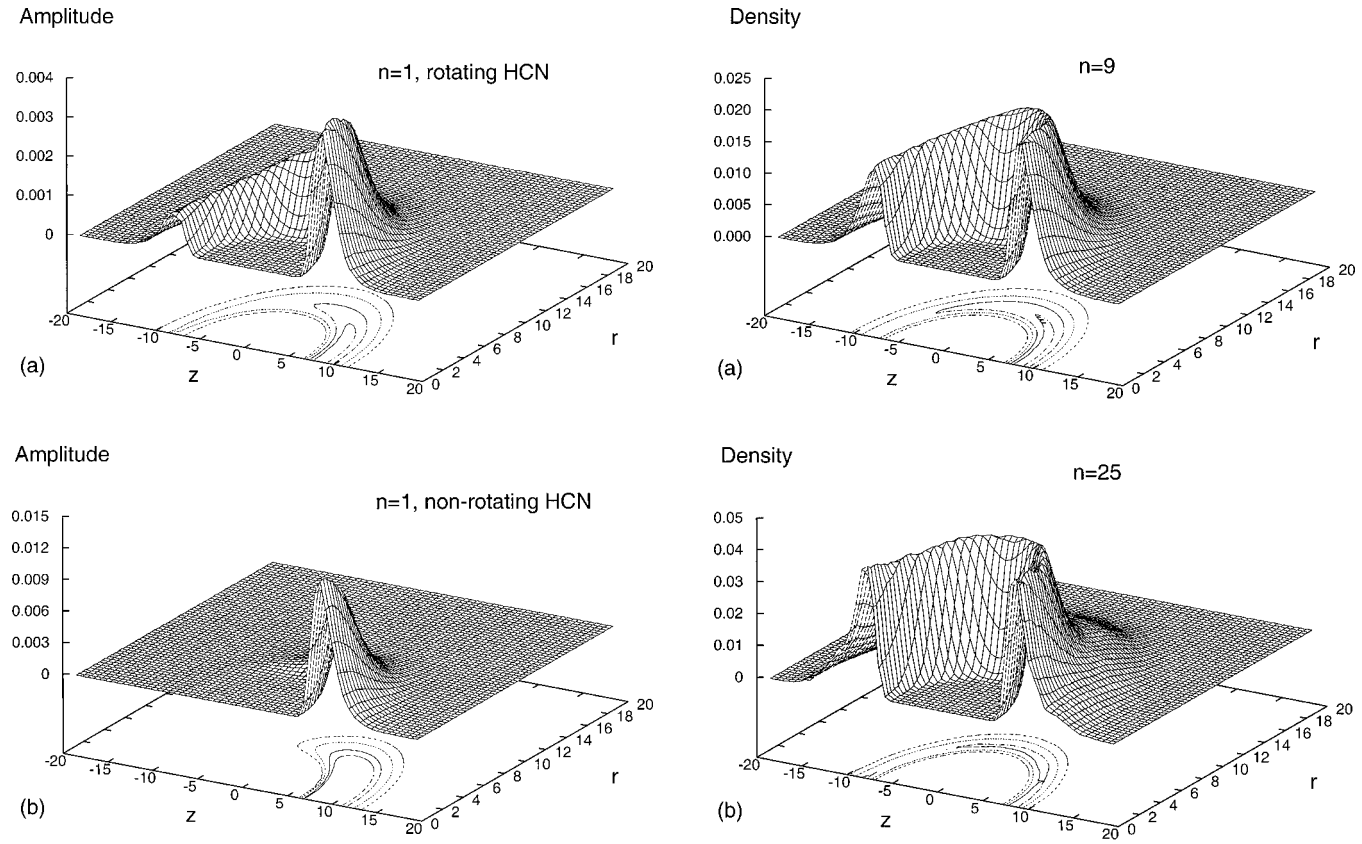

FIG. 2. Two-dimensional representation of the ground state wave function Ψ of the HCN–He $n=1$ dimer. Ψ was computed with unbiased DMC here. The rotation of the HCN molecule is included in (a), whereas (b) corresponds to a nonrotating (but translating) HCN molecule. The origin is set at the molecular center of mass. The HCN molecule is oriented as N–C–H, the H atom being at positive *z*. All distances are in atomic units. The normalization of the amplitude is arbitrary but identical in both figures.

FIG. 3. Ground state helium density for: (a) HCN He_9, (b) HCN He_{25}, (c) HCN He_{60}. The mixed densities are shown here, i.e., $\rho_{\text{mixed}}=\langle\Psi|\hat{\rho}|\Psi_T\rangle$. The orientation of the HCN molecule is identical to that defined in Fig. 2.

$n=9$, 25, and 60, respectively, for the true physical system (i.e., with the HCN rotational kinetic energy included). The comparison of the wave function for one helium atom [Fig. 2(a)] with the density for $n=9$ helium atoms [Fig. 3(a)] and for $n=25$ [Fig. 3(b)] shows that the angular dependence of the maximum on the elliptical-like contours around the molecule tends to smooth out as n increases. For large clusters, $n>20$, the helium environment around HCN becomes thus more isotropic than was observed for the more strongly bound molecules like SF_6 (Ref. 8) and OCS (Ref. 3). This results from the smaller anisotropy in the He–HCN interaction potential. For more than $n\sim 17-20$ helium atoms, a second solvation shell is evident in the mixed densities, as Fig. 3(c) shows for a cluster with $n=60$ helium atoms.

B. HCN–He$_n$ excited states from fixed node

Experiments in doped helium clusters show that the rotational spectrum of HCN inside ^{4}He clusters possesses the same symmetry as in gas phase, but that the effective rotational constant is reduced by ~19%.[4,5] This reduction is considerably less than the ~65% reduction seen for more strongly bound species such as SF_6.[6] As noted above, the study of excited states within the fixed node approximation requires some estimate of the nodal structure. Insight into this can be obtained from level assignments made according to simple models. Previous studies of SF_6 in ^4He_n (Refs. 3 and 8) present rotational levels corresponding to $J\sim j$, where J is the total angular momentum, and j the molecular angular momentum. Those calculations were based on the nodal structure for a free spherical top $D^1_{00}(\alpha,\beta,\gamma)$, α, β, γ being the Euler angles describing the orientation of the principal axis frame of the molecule in space fixed frame. This function is proportional to

$$\Psi^{(1)}_{\text{node}}(\mathcal{R})=\cos(\beta). \tag{27}$$

In the particular case of the smallest cluster HCN–He, with $n=1$, we have used collocation calculations of Atkins and Hutson[14] in order to analyze the exact eigenfunctions

TABLE III. Ground and rotationally excited energy levels for HCN–He, reported in cm^{-1}. The level assignments are the zeroth order level assignments $|jlJ\rangle$ originally made in Ref. 36 and followed by Ref. 14.

	E_0	$\cos(\theta+\chi)$	$\cos[(\theta_{HCN}+\theta_{He})/2]$	$\cos(\beta)$
DMC	-9.71 ± 0.14	-5.84 ± 0.2	-9.04 ± 0.2	-7.25 ± 0.2
Collocation method (Ref. 14)	-9.657	-5.899	-9.127	N/A
Level assignment (Ref. 14)	$\|000\rangle$	$\|110\rangle$	$\|011\rangle$	N/A

and to test both this free molecule nodal structure and two other nodal approximations. The level which has been assigned[14,36] as $|j=1, \ell=1, J=0\rangle$ shows a single nodal surface that is approximately r-independent.[15] (In this assignment scheme, J is the total rotational quantum number, j the quantum number of HCN, which is to a good approximation conserved in the weakly bound complex, and ℓ an ''orbital'' quantum number associated with the rotation of the helium around the HCN.) This motivated us to use a trial nodal surface for the $|110\rangle$ state that is defined by

$$\Psi^{(2)}_{\text{node}}(\mathcal{R}) = \cos(\theta+\chi), \tag{28}$$

where χ is a parameter and θ is the internal Jacobi angle of the cluster. A third trial nodal surface was motivated by the fact that the potential is minimum when the He atom is aligned with the HCN molecule. This corresponds to $\theta_{HCN} = \theta_{He}$, where θ_M is the spherical polar angle in the arbitrary space fixed frame. Consequently, a probable position of a node is a perpendicular surface to $\theta_{HCN} = \theta_{He}$; namely,

$$\Psi^{(3)}_{\text{node}}(\mathcal{R}) = \cos\left[\frac{\theta_{HCN}+\theta_{He}}{2}\right]. \tag{29}$$

For each of these three nodal structures, we performed importance sampling DMC runs restricted to each one of the two sides of the node, i.e., using $\Psi^{(0)}_T(R,\theta)\Psi^{(i)}_{\text{node}}(\mathcal{R})$ as a guiding function, for $i=1,2,3$. Those calculations were done with approximately 5000–6000 walkers. After equilibration of the configuration, we perform one run of 800 blocks, each of which consist of 150 time steps with $\delta\tau=10$ a.u. The optimal parameter value for the second node $\Psi^{(2)}_{\text{node}}(\mathcal{R})$ was found to be $\chi=15.65$ deg. For the other two trial nodal surfaces, both runs restricted to one sign of $\Psi^{(i)}_{\text{node}}$ gave the same energy. The results are summarized in Table III, where they are compared with the corresponding values from collocation calculations and level assignments to the zeroth order states $|jlJ\rangle$ made in Refs. 14 and 36.

For two of the nodal structures tested for $n=1$, namely for $\Psi^{(2)}_{\text{node}}$ and $\Psi^{(3)}_{\text{node}}$, the DMC results are in agreement with the collocation values,[14] attesting that the trial nodes used are relevant and accurate. These levels correspond to the zeroth order assignments $|110\rangle$ and $|011\rangle$, respectively, according to the weak coupling classification of Refs. 36 and 14. Note that according to these zeroth order assignments, only one of these two levels has total cluster angular momentum J greater than zero, i.e., $|011\rangle$. The experimental observation of transitions to this level (and to a level assigned as $|022\rangle$) was used in Ref. 36 to obtain a fitted rotational constant of $B = 0.264\,cm^{-1}$ for the HCN–He complex.

In contrast to this excellent agreement between DMC and collocation results for the trial nodal surfaces $\Psi^{(2)}_{\text{node}}$ and $\Psi^{(3)}_{\text{node}}$, the nodal surface in the space fixed frame, $\Psi^{(1)}_{\text{node}}$, leads to an excitation of $-7.25\pm0.2\,cm^{-1}$, which has no counterpart in the levels obtained by the collocation scheme. This proves that this space fixed node is incorrect for $n=1$, and has no physical meaning for the HCN–He dimer. We note that an energy level with the free rotor nodal structure might be given the zeroth order level assignment $|jlJ\rangle = |101\rangle$. References 14 and 36 gave this assignment to a much higher-lying energy level, lying just below the level derived from $\Psi^{(2)}_{\text{node}}$. It is quite revealing that the minimum energy derived from the free molecule, space fixed nodal surface bears no relation to the energy of this experimentally assigned $|101\rangle$ level. This indicates HCN is really not at all in a weak coupling limit, and that the zeroth order level assignments should be treated with caution.

For larger clusters, $n>1$, collocation and basis set methods are not feasible, and only DMC methods can then provide access to excited states. The accuracy of the nodal approximations for larger size clusters is not necessarily the same as that for $n=1$, since the helium density around the molecule changes as n increases. As noted above, it becomes considerably more symmetrical, suggesting that the space fixed nodal approximation might become more accurate at larger sizes. Therefore we have analyzed the evolution of the corresponding energy as the number of helium atoms increases, motivated by the expectation that this node should be more physical for a cluster in which the helium density is more symmetric around HCN than in the HCN–He dimer. Since the angular dependence for larger clusters tends to smooth out, we employ the radial trial wave function, i.e., $\Psi^{(e)}_T = \Psi^{\text{rad}}_T(R)\Psi^{(1)}_{\text{node}}$. The energy value for $n=1$ is unaffected by this change of trial wave function. We present the n dependence from this trial function in Fig. 4. This plot corresponds to the evolution of the difference between the excited and the ground state energies, which is assigned as twice the effective rotational constant, B. In order to obtain a relatively small error bar, we used up to 80 000 walkers and perform these calculations on parallel computers, scattering the walkers onto the different processors. By looking at the fixed node energies, we would conclude that B appears to saturate with just three helium atoms. However, this nearly constant fixed node value lies below the experimental value measured for $n\geqslant10^3$ helium atoms. The computation of larger cluster sizes within the fixed node approximation was not pursued since a further reduction of the error bars becomes intractable. While this could, in principle, be overcome by the implementation of correlated sampling,[31,42] implementation of this is not straightforward here since the two states of interest have a different nodal structure. A procedure such as the one proposed by Filippi and Umrigar[43] for

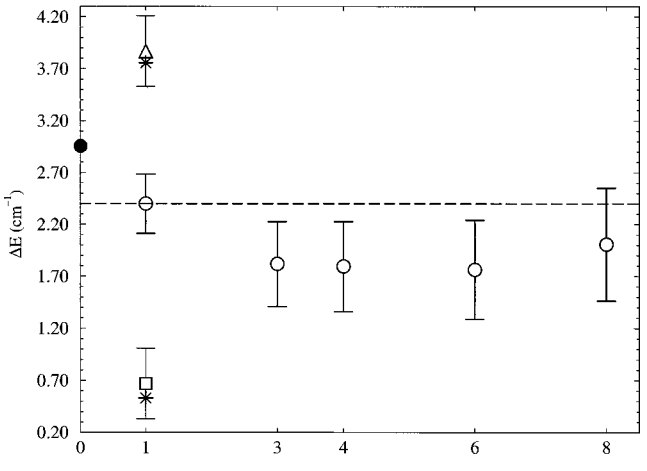

FIG. 4. Evolution of the fixed node excitation energy $\Delta E = E^{(e)} - E^{(0)}$ with the number of helium atoms n (open circles). The space fixed trial nodal surfaces $\Psi^{(1)}_{\text{node}}$ were employed here, Eqs. (26) and (27). The corresponding experimental values for HCN in the gas phase (Ref. 36) (solid circle) and for HCN inside large ^{4}He clusters (Ref. 4) (dashed line) are also shown. For $n=1$ we also show the excitations obtained from nodal trial functions $\Psi^{(2)}_{\text{node}}$, Eq. (28) (open triangle) and $\Psi^{(3)}_{\text{node}}$, Eq. (29) (open square). The collocation energy levels corresponding to these excitations are shown as asterisks. They correspond, respectively, to the zeroth order level assignments $|110\rangle$ and $|011\rangle$ of Refs. 36 and 14.

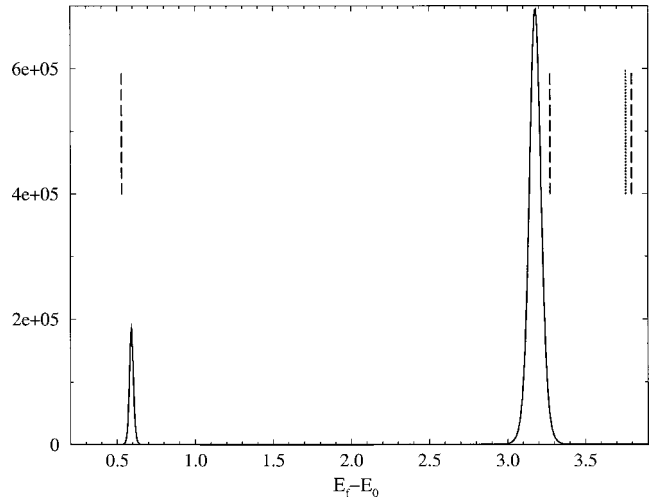

FIG. 5. POITSE excitation spectrum for the HCN–He dimer, obtained using $\cos(\beta)$ as a projector. Vertical lines correspond to the collocation results from Ref. 14 for $J=0$ (dotted line) and $J=1$ (dashed lines).

this situation may lead to significant trial wave function bias.

These results suggest that the free molecule spatial nodal structures do not correspond to the true nodal structures of the rotational excitations in larger helium clusters. In the next section we calculate excitation energies without any fixed nodal constraint, and will see that the corresponding nodal structures can be quite different from the free molecule nodal surfaces. The underlying cause of this lack of accuracy of a free molecule description may be the unusual energetics of the HCN–He dimer, that we have commented on earlier (Sec. I). Due to the close energetic proximity of the ground state and the potential barrier in the HCN–He dimer, there may be an enhancement of the coupling between the rotational and translation degrees of freedom of HCN in $^4\text{He}_N$, by quantum reflection at the potential barrier.

C. HCN–He$_n$ excited states from POITSE

Given the uncertainties of the fixed node approximation illustrated above, we now apply the POITSE methodology to the rotational excitations of HCN. POITSE has been shown to lead to exact excited state energies when no knowledge of the *exact* nodal surface is available but when a "good" estimate of it is accessible.[18] This is precisely the situation here, where the rotational excitation is located primarily on the molecule. The molecular rotation function $A=\cos(\beta)$, i.e., the $J=1$, $M=0$, $K=0$ Wigner function, will therefore be used as projector here. This function is one of the three basis set functions $|J,0,M\rangle$, $J=1$, $M=0,\pm 1$ which are used to describe a rotating linear rigid object with one quantum of excitation.[44] We thus expect to project the ground state wave function onto a linear combination of the true $J=1$ states. We already know that for $n=1$, the projector $A=\cos(\beta)$ will not yield a single peak, otherwise the fixed node calculation described above would have given a correct value.

The spectrum for the $n=1$ HCN–He dimer obtained from 1056 POITSE decays terminated at $\tau_{\text{final}} = 693\,000$ a.u., is presented in Fig. 5. We used 5000 walkers and a time step of 20 a.u. This POITSE spectrum is converged with respect to the number of POITSE decays. The guiding function used here is the radial one, Eq. (25). The anisotropic trial function Eq. (21) leads to a similar spectrum. Figure 5 shows a two peak structure, i.e., this projector accesses at least two excited states. This confirms our initial expectation based on the failure of the fixed node approximation using the space fixed node, Eqs. (26) and (27). Neither of the two peaks obtained correspond to that fixed node result. Instead, the excitation energies are in good agreement with the exact values computed by the collocation method and listed in Table III. Moreover, it can be seen by comparison with all the collocation energy levels listed in Ref. 14 that only $J=1$ states are probed with this particular projector. The maxima of both peaks are within 10% of the "exact" values (relative error). The statistical noise inherent to the Monte Carlo scheme, as well as the presence of multiple decays in the projection which makes the realization of the inverse Laplace transform more delicate,[17] is responsible for this uncertainty.

We now proceed to examination of the evolution of these $J=1$ states as the number of helium atoms in the cluster, n, increases. Figures 6(a)–6(c) show POITSE spectra for various cluster sizes ranging from $n=1$ to $n=25$. For these calculations, the number of walkers was reduced to 2000 and the number of decays was increased by $\sim$100, until the position of the maximum of the first peak is unchanged. The reduction from 5000 to 2000 walkers does not notably affect the $n=1$ spectrum. The time step is the same as in the $n=1$ case and the final number of decays was around 1000 for all sizes presented. The effect is that we reduce the computational effort for the larger sizes without loosing any convergence with respect to the number of decays included in the POITSE average. The decay length was shortened to $\tau_{\text{final}} = 494\,800$ a.u. for $n=15$, and to $\tau_{\text{final}} = 395\,740$ a.u. for

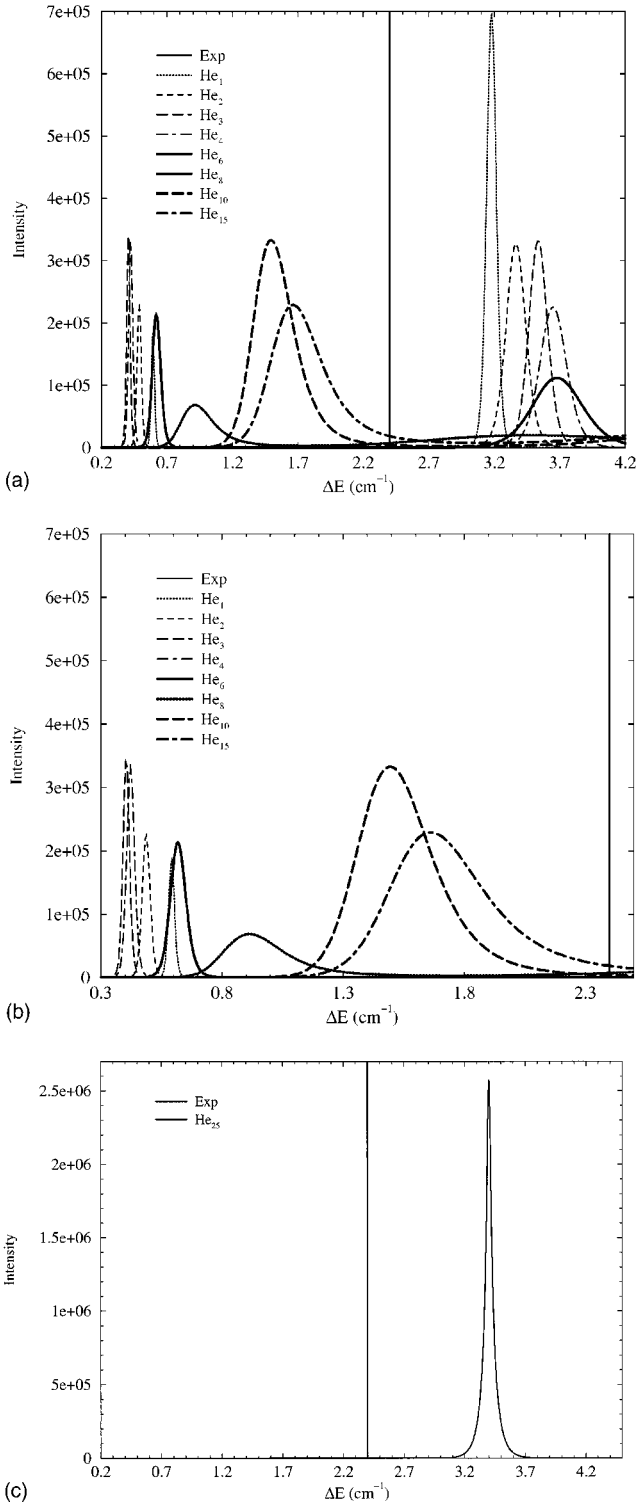

FIG. 6. POITSE excitation spectra for HCN He_n, obtained using $\cos(\beta)$ as a projector. The vertical line corresponds to twice the experimentally measured rotational constant for HCN ($v=0$) in large helium clusters (Ref. 4) $2B=2.40\ cm^{-1}$. (a) Spectra for $n=1-15$, showing two peaks. (b) Magnification of the first peak for $n=1-15$. (c) Spectrum for $n=25$, showing only a single peak.

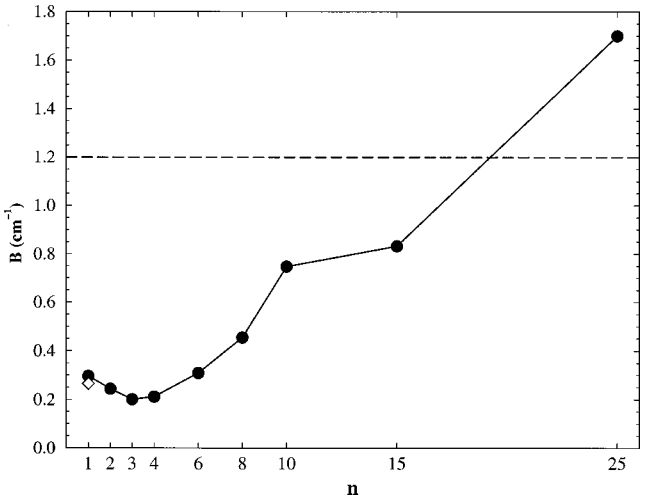

FIG. 7. Effective rotational constant B extracted from the first, low energy, POITSE peak for each n in Fig. 6. The experimental rotational constants for $n=1$ (diamond, Ref. 36) and for $n\simeq3000$ (dashed line, Ref. 4) are also shown.

$n=25$. This was done to obtain greater efficiency at the larger sizes, since as n increases, the energy difference probed increases. Consequently, the exponential decay has a shorter time constant and need not be followed for such long imaginary times. For the largest cluster size studied ($n=25$) the number of walkers was reduced to 1000. In order to perform these $(3n+5)$-dimension calculations, we used a parallel POITSE code which scatters the computation of the decays onto different processors. The code is obviously perfectly suitable for parallelization and is highly scalable. The largest cluster calculations were performed on an IBM/SP2 power 3 (NPACI Blue Horizon parallel machine). The CPU requirement varies as approximately 1:1.7:4.7:6.7:13.4:34 for $n=1:4:8:10:15:25$. These sizes correspond to systems having 8:17:29:35:50:80 degrees of freedom, respectively. This is the first application of POITSE to a truly large multidimensional cluster system.

For sizes $n=1-15$, the POITSE spectrum consists of two peaks, shown in Fig. 6(a). For the largest size studied, $n=25$, the spectrum is made of only one broad peak, shown in Fig. 6(c). The width of these peaks increases with the number of helium atoms n. We can tentatively attribute this trend to the inherent increase with n of the statistical noise in the DMC procedure. However, as previously discussed,[17] the width of the spectral peaks after inversion is not related to the accuracy of the derived excitations in any obvious manner. For all sizes shown in Fig. 6(a), the lower energy peak is narrower than the higher energy one. Figure 6(b) presents a magnification of the first peak for $n=1-15$. It can be seen that the position of this peak first decreases when the number of helium atoms increases from 1 to 3, and then turns around and increases with further increase in n. Even if the precise location of the peaks are subject to a similar error as that in the $n=1$ spectrum, it is evident that for, e.g., $n=8$, the first energy difference is definitively larger than the corresponding difference for $n=1$. For reference, we indicate with the vertical line in Figs. 6(a)–6(c) the position of the lowest rotational level predicted by the experimental measurements of B for HCN inside large helium clusters,[4] i.e., $E\equiv2B=2.40\ cm^{-1}$.

Figure 7 presents the extracted B values obtained from the first POITSE peak, as a function of the number of helium atoms n. Also shown are the experimental values for both

$n=1$ (0.264 cm^{-1}, measured in Ref. 36) and inside large ^4He clusters (1.204 cm^{-1}, measured in Ref. 4). The peaks for the two largest cluster sizes presented here, $n=15$ and $n=25$, lie below and above the experimental value, respectively. This oscillatory behavior shows that a cluster with 15 or 25 helium atoms is still not large enough to faithfully represent the local environment controlling the rotational dynamics of HCN in the experimental clusters, for which the average size is a few thousand.[4,5] The reason why the effective B value extracted from the $n=25$ cluster is higher than the experimental value for much larger clusters ($n \geqslant 10^3$) is not totally understood at this time. Two possible explanations can be advanced. The first one derives from consideration of the physics. As seen from the density radial profiles presented in Fig. 1, the asymptotic structure of the helium solvation layers around HCN is not yet completed for a size of even $n=30$ helium atoms. We might thus expect that the position of the peak is not yet located at its final saturation position as a function of cluster size n. The second possible explanation is that the $n=25$ POITSE spectrum is not completely converged with respect to the total decay time. While this spectrum is, like those in Fig. 6(a), converged with respect to the number of POITSE decays included in the averaging procedure, the decay length for $n=25$ was shortened to a smaller value of the total imaginary time, for the reasons noted above. If this decay length is not asymptotic, there could be some possible underlying structure of the broad peak observed. Computational constraints precluded more extensive calculations for the $n=25$ cluster to test whether there might indeed be a spectral contribution from the residual decay at longer times.

Finally, we reiterate that the fixed node saturation B value would lead to an excitation at 1.8 cm^{-1}. As stated earlier, this is not in agreement with the experimental value obtained in much larger clusters. Figure 6 shows that it is also not reproduced by the POITSE spectra for these cluster sizes. Thus the POITSE excitations also do not correspond to the free molecular nodal structure, although the fact that they are arrived at from a free molecular projector does imply that they may have some overlap with these. The results for $n=1$ give confidence in the accuracy of the POITSE excitations, allowing us to strengthen our physical conjecture that the slow approach of the rotational excitations of HCN in ^4He clusters is related to the unusual confluence of energetic and quantum influences deriving from the location of the zero point energy of HCN–He close to the potential barrier.

IV. CONCLUSION

We have presented quantum Monte Carlo studies of HCN He_n in its ground and low-lying excited rotational states, where the rotational excitation is localized at least partly on the molecule. Comparison of ground state wave functions for the real (rotating) system with those calculated for a model reference where the HCN is artificially constrained not to rotate, show explicitly that there is no significant extent of any adiabatic following by helium atoms with the rotational motion of this molecule. This is consistent with previous predictions based on simple classical estimates showing that this molecule rotates too fast and the potential asymmetry is too weak, for the helium density to adiabatically move with the molecule.[3] In quantum mechanical terms, this can be understood in terms of the close energetic proximity of the ground state of the He–HCN dimer to the potential barrier separating the two different orientational minima (Sec. I).

The excited state calculations within fixed node approximations show that the nodal structure of excited states for small clusters is very different from that seen with the more strongly bound and slower, spherical top rotor, SF_6. In particular, for HCN, the free molecule spatial nodal approximations were seen to be noticeably inaccurate at small sizes ($n=1-10$), although they have been shown to provide very accurate results for SF_6.[8] We have used the $n=1$ HCN–He dimer, for which exact energies can be obtained from the collocation approach, to explicitly expose the general limitation of the fixed node approach, showing that it leads to an erroneous energy level when the incorrect node is used. From a physical perspective, this nodal finding for HCN is extremely interesting since the free molecule nodal structure is what one might naively expect to be appropriate for larger clusters possessing a more symmetric local solvation environment. The ellipsoidally symmetric solvation shell of helium in the first shell around HCN is therefore providing a sufficient level of hindrance to the molecular rotation to cause the nodal surfaces for rotation to be modified in their symmetry. This may also be a consequence of the very close match between the ground state of HCN–He, and the potential barrier between the two orientational minima.

The problems associated with the fixed node approximation were shown here to be surmountable by using the intrinsically exact POITSE method. This was demonstrated first for the $n=1$ HCN–He dimer by comparison of the POITSE excitations with results from calculations with the collocation method. Most significant here was the finding that the space fixed projector yielded accurate POITSE excitation energies, while a fixed node calculation with the corresponding space fixed nodal structure failed completely to provide an adequate representation. The good agreement between POITSE and collocation results obtained for $n=1$ provides confidence for the accuracy of the POITSE spectra obtained for larger clusters. One of the excitations derived from the space fixed projector appears to evolve to the experimental rotational constant measured in larger clusters, but in a relatively slow and nonmonotonic fashion. Calculations on larger clusters would be desirable to provide conclusive confirmation of this nonmonotonic convergence to the saturation value.

Overall, the results for HCN rotations in helium clusters composed of the boson isotope ^4He are striking in their slow rate of convergence to a cluster rotational constant that is independent of further increase in cluster size. This suggests that HCN lies in a critical region of the parameter space, highlighted by the energetics of the HCN–He dimer mentioned above, in which the quantum rotational dynamics are highly sensitive to small modifications of the helium density as additional helium atoms are attached to these clusters over the size range $n=1-30$. This sensitivity to cluster size over

the small size range is very different from the behavior observed for the heavier molecules SF_6 (Ref. 3) and OCS.[45] For these heavier molecules the rotational constant decreases monotonically from the gas phase value to a saturation value that is reached at a very small number of atoms (8 for SF_6 and 5–6 for OCS), and then remains constant.[3] The value of n at saturation is approximately equal to the number of ^{4}He atoms that can be packed into the positions of the global potential minima. This heavy molecule behavior is consistent with the dynamics of an adiabatically following local nonsuperfluid density that constitutes only a fraction of the first solvation shell.[3] In contrast, for HCN the rotational constant shows a nonmonotonic dependence on n, and does not appear to have reached saturation at even a complete solvation shell.

These marked differences for the rotational dynamics of HCN in helium clusters from both that of the heavier molecules SF_6 and OCS, and that of lighter molecules such as HF (Sec. I) appears to reflect a critical balance between the molecular rotational motion and its translational motion, at energies just above the potential barriers of the HCN–He system. Strong quantum coupling effects are introduced by the close proximity of the zero point energy to the potential barrier in the HCN–He system. These will be amplified in the larger clusters, with some modifications by the additional He–He correlations. This special energetic feature of the HCN–He system appears to underly all three dynamic characteristics observed here, namely, (i) the rotational nodal structure, (ii) the nonmonotonic and slowly varying size dependence of the rotational constant, and (iii) the lack of adiabatic following of helium with the HCN rotation.

ACKNOWLEDGMENTS

The authors acknowledge financial support from the National Science Foundation through NSF Grant No. CHE-9616615. Supercomputer time was made available through a National Partnership for Advanced Computational Infrastructure (NPACI) program of NSF, administered by the San Diego Supercomputer Center.

[1] J. P. Toennies and A. F. Vilesov, Annu. Rev. Phys. Chem. **49**, 1 (1998).
[2] K. B. Whaley, *Advances in Molecular Vibrations and Collision Dynamics, Vol. III*, edited by J. Bowman and Z. Bačić (Academic, New York, 1998), pp. 397–451.
[3] Y. Kwon, P. Huang, M. V. Patel, D. Blume, and K. B. Whaley, J. Chem. Phys. **113**, 6469 (2000).
[4] A. Conjusteau, C. Callegari, I. Reinhard, K. K. Lehmann, and G. Scoles, J. Chem. Phys. **113**, 4840 (2000).
[5] K. Nauta and R. E. Miller, Science **283**, 1895 (1999).
[6] M. Hartmann, R. E. Miller, A. F. Vilesov, and J. P. Toennies, Phys. Rev. Lett. **75**, 1566 (1995).
[7] S. Grebenev, M. Hartmann, M. Havenith, B. Sartakov, J. P. Toennies, and A. F. Vilesov, J. Chem. Phys. **112**, 4485 (2000).
[8] E. Lee, D. Farrelly, and K. B. Whaley, Phys. Rev. Lett. **83**, 3812 (1999).
[9] Y. K. Kwon and K. B. Whaley, Phys. Rev. Lett. **83**, 4108 (1999).
[10] C. Callegari, A. Conjusteau, I. Reinhard, K. K. Lehmann, and G. Scoles, Phys. Rev. Lett. **83**, 5058 (1999).
[11] D. Blume, M. Lewerenz, F. Huisken, and M. Kaloudis, J. Chem. Phys. **105**, 8666 (1996).
[12] K. Nauta and R. E. Miller, Science **287**, 293 (2000).
[13] R. Moszynski, P. E. S. Wormer, B. Jeziorski, and A. V. der Avoird, J. Chem. Phys. **101**, 2811 (1994).
[14] K. M. Atkins and J. M. Hutson, J. Chem. Phys. **105**, 440 (1996).
[15] A. Viel, M. V. Patel, P. Niyaz, and K. B. Whaley, Comput. Phys. Commun. (in press, 2001); preprint at physics/0109004 at http://xxx.lanl.gov
[16] D. Blume, M. Lewerenz, P. Niyaz, and K. B. Whaley, Phys. Rev. E **55**, 3664 (1997).
[17] D. Blume, M. Lewerenz, and K. B. Whaley, J. Chem. Phys. **107**, 9067 (1997).
[18] D. Blume, M. Mladenović, M. Lewerenz, and K. B. Whaley, J. Chem. Phys. **110**, 5789 (1999).
[19] D. Blume and K. B. Whaley, J. Chem. Phys. **112**, 2218 (2000).
[20] P. Huang, A. Viel, and K. B. Whaley, in *Recent Advances in Quantum Monte Carlo Methods, Part II* (World Scientific, New York, 2001).
[21] P. Huang and K. B. Whaley, to be published (2001).
[22] M. A. Suhm and R. O. Watts, Phys. Rep. **204**, 293 (1991).
[23] V. Buch, J. Chem. Phys. **97**, 726 (1992).
[24] C. J. Umrigar, M. P. Nightingale, and K. J. Runge, J. Chem. Phys. **99**, 2865 (1993).
[25] B. L. Hammond, W. A. Lester, and P. J. Reynolds, *Monte Carlo Methods in Ab Initio Quantum Chemistry* (World Scientific, Singapore, 1994).
[26] K. B. Whaley, Int. Rev. Phys. Chem. **13**, 41 (1994).
[27] N. Metropolis *et al.*, J. Chem. Phys. **21**, 1087 (1953).
[28] C. J. Umrigar, K. G. Wilson, and J. W. Wilkins, Phys. Rev. Lett. **60**, 1719 (1988).
[29] R. Assaraf, M. Caffarel, and A. Khelif, Phys. Rev. E **61**, 4566 (2000).
[30] R. N. Barnett and K. B. Whaley, Phys. Rev. A **47**, 4082 (1993).
[31] M. Lewerenz, J. Chem. Phys. **104**, 1028 (1996).
[32] M. A. McMahon, R. N. Barnett, and K. B. Whaley, J. Chem. Phys. **99**, 8816 (1993).
[33] H. S. Lee, J. M. Herbert, and A. B. McCoy, J. Chem. Phys. **110**, 5481 (1999).
[34] J. Casulleras and J. Boronat, Phys. Rev. B **52**, 3654 (1995).
[35] R. A. Aziz, F. R. W. McCourt, and C. C. K. Wong, Mol. Phys. **61**, 1487 (1987).
[36] S. Drucker, F. M. Tao, and W. Klemperer, J. Phys. Chem. **99**, 2646 (1995).
[37] R. E. Grisenti, W. Schöllkopf, J. P. Toennies, G. C. Hegerfeldt, T. Köhler, and M. Stoll, Phys. Rev. Lett. **85**, 2284 (2000).
[38] C. Leforestier, J. Chem. Phys. **94**, 6388 (1991).
[39] M. Lewerenz, J. Chem. Phys. **106**, 4596 (1997).
[40] R. N. Barnett and K. B. Whaley, J. Chem. Phys. **99**, 9730 (1993).
[41] M. V. Patel, A. Viel, F. Paesani, and K. B. Whaley, J. Chem. Phys. (to be published).
[42] B. H. Wells, Chem. Phys. Lett. **115**, 89 (1985).
[43] C. Filippi and C. J. Umrigar, Phys. Rev. B **61**, R16291 (2000).
[44] R. N. Zare, *Angular Momentum* (Wiley Interscience, New York, 1988).
[45] F. Paesani, A. Viel, F. Gianturco, and K. B. Whaley, J. Chem. Phys. (to be published).